Applied Catalysis B: Environmental 179 (2015) 139–149

Contents lists available at ScienceDirect

Applied Catalysis B: Environmental

journal homepage: www.elsevier.com/locate/apcatb

Influence of the niobium supported species on the catalytic dehydration of glycerol to acrolein

C. García-Sancho, J.A. Cecilia, A. Moreno-Ruiz, J.M. Mérida-Robles, J. Santamaría-González, R. Moreno-Tost*, P. Maireles-Torres

Universidad de Málaga, Departamento de Química Inorgánica, Cristalografía y Mineralogía (Unidad Asociada al ICP-CSIC), Facultad de Ciencias, Campus de Teatinos, 29071 Málaga, Spain

ARTICLE INFO

Article history:
Received 6 February 2015
Received in revised form 27 April 2015
Accepted 6 May 2015
Available online 12 May 2015

Keywords:
Niobium
Acrolein
Glycerol
Dehydration
Acid catalysts

ABSTRACT

The present work deals with the catalytic performance of a series of supported niobium oxide (1–12 wt% Nb_2O_5) catalysts in the gas phase dehydration of glycerol. The niobium species were supported on a mesoporous zirconium doped silica (Si/Zr molar ratio of 5) by incipient wetness impregnation. The catalysts were characterized by means of XRD, N_2 adsorption, NH_3–TPD, Raman spectroscopy, adsorption of pyridine coupled to FTIR spectroscopy and XPS. The catalytic reaction was carried out in gas phase at 325 °C. The support exhibits the highest glycerol conversion (91 mol%) after 2 h, but it is less selective to acrolein (25 mol%). The supported niobium species do not ameliorate the glycerol conversion, but the acrolein selectivity is markedly improved, attaining a value of 45 mol% after 2 h for the catalyst with 8 wt% of Nb_2O_5. This catalyst can be regenerated by thermal treatment under an air flow for 4 h, although the regeneration causes a lowering of the Brönsted/Lewis acid sites ratio, thus decreasing the selectivity toward acrolein.

1. Introduction

Nowadays, society is experiencing a growing concern about the impact of human activity on the environment. Many of the problems associated with deterioration of air quality are related to the excessive use of fossil fuels, which has led to a notable increase of emissions of greenhouse gases and pollutants. In this sense, currently, much attention is being paid to the development of renewable sources for production of energy and chemicals, aiming to fossil fuels replacing.

Concerning transportation liquid fuels, it is feasible to substitute and mix gasoline and diesel with bioethanol and biodiesel, respectively. However, most of the current feedstocks for the production of these two biofuels compete with the food industry, consequently affecting to the world market price of such raw materials. In this scenario, for instance, second-generation biodiesel production involves the use of triglycerides derived from *Jatropha curcas* [1–3], microalgae [4], or waste cooking oils [5].

The worldwide production of biodiesel has also generated an important surplus of glycerol, as byproduct of this oleochemical industry [6]. To date, glycerol finds applications in cosmetics, pharmaceuticals, tobacco industry, among others, up to reach more than 1500 direct applications [7]. However, it has not been used as raw material for the synthesis of other chemicals due to the high price of refined glycerol. Nevertheless, as a consequence of the outbreak of biodiesel production, the glycerol price has experienced a drastic decline, thus, opening the possibility to use it for the synthesis of a large spectrum of chemicals.

In this context, acrolein has attracted considerable attention of many research groups because of its many industrial applications, among which are the synthesis of acrylic acid (precursor of acrylic polymers), *L*-methionine (essential aminoacid used in animal feeding), among others. Currently, acrolein is obtained in the petrochemical industry from the partial oxidation of propene. Therefore, there is a great deal of interest in the production of acrolein from a renewable source (glycerol), developing a greener and environmentally friendly process along with an economic improvement in the oleochemical platform.

Initially, the synthesis of acrolein from glycerol was studied in aqueous phase, under sub-supercritical and supercritical conditions, using homogeneous catalysts [8,9]. This process presents several technical and environmental problems, which have led to be discarded and replaced by the gas phase reaction, under heterogeneous catalysis. Gas phase dehydration of glycerol to acrolein

* *Corresponding author. Tel.: +34 952132021; fax: +34 952131870.
E-mail address: rmtost@uma.es (R. Moreno-Tost).

http://dx.doi.org/10.1016/j.apcatb.2015.05.014
0926-3373/

has been carried out in the presence of different solid acid catalysts, such as zeolites [10–14], heteropolyacids [15–19], tungsten oxide [20–26], mesoporous silica with anchored sulphonic groups [27] or doped with heteroatoms [28,29], phosphate impregnated metal oxides [30], sulfated zirconia [31] and mixed oxides [32–37]. Moreover, the interest of the industry in the dehydration of glycerol is demonstrated by the numerous patents devoted to this reaction [38–42]. On the other hand, the main drawback of many catalysts evaluated in the gas-phase dehydration of glycerol is their deactivation with time on stream [43–45]. However, lately, some promising catalytic systems have been developed showing a suitable stability [26,32,46].

Among solid acid catalysts, niobium based catalysts are water-tolerant, and they have been used in aqueous media to obtain valuable chemicals from biomass. Thus, they have been also tested in the dehydration of glycerol to acrolein [36,45,47–49]. Chai et al. [45] employed amorphous niobium oxide, evaluating the impact of calcination temperature of $Nb_2O_5{\cdot}nH_2O$ on the catalytic activity. The calcination treatment affected to the acid strength distribution and hence to the glycerol conversion and acrolein selectivity. An amorphous catalyst, prepared after calcination at 400 °C, showed the highest glycerol conversion (88 mol%) and acrolein selectivity (51 mol%). The effect of calcination temperature was also studied by Shiju et al. [47] for niobia supported on silica catalysts, and they found that glycerol conversion and acrolein selectivity increased with the niobia loading, reaching the highest values (70 and 65 mol%, respectively) for a catalyst with 20 wt% Nb_2O_5, calcined at 400 °C. However, higher calcination temperatures led to lower glycerol conversion and acrolein selectivity values. This behavior was attributed to the higher acid strength of catalysts calcined at lower temperatures. In these two aforementioned works, the niobia catalysts showed initial glycerol conversion close to 100%, but it decreased rapidly with time-on-stream. Nevertheless, catalysts fully recovered the initial catalytic activity after an oxidation treatment under an oxygen flow.

Massa et al. [48] have evaluated the catalytic behavior of niobia supported on alumina, silica and titania, at a reaction temperature of 305 °C, studying the influence of niobia dispersion on the catalytic performance. Thus, niobia supported on SiO_2 was the least selective to acrolein because of the existence of crystalline Nb_2O_5 particles. The authors attributed the acrolein formation to the presence of Brönsted acid sites, whereas hydroxyacetone was correlated to the Lewis acid sites. Moreover, they demonstrated that oxygen co-feeding reduced the deactivation process, since the formation of coke precursors was inhibited.

On the other hand, niobium supported on ZrO_2 [20] attained an acrolein yield of 75%, with full glycerol conversion at 305 °C. Raman and FTIR spectroscopies have allowed concluding that superficial polymeric structures with Nb–OH Brönsted acid sites were the most selective to acrolein. It was not observed any synergistic effect when niobia was co-supported with tungsten.

Niobium was also studied as mixed oxides with zirconium [32,36] and tungsten [21]. Lauriol-Garbay et al. [32,36] found that mixed oxides were very stable with time-on-stream, attaining glycerol conversion of 82% and acrolein selectivity of 72%, after 177 h at 300 °C. The selectivity to acrolein was attributed to the presence of weak or moderate Brönsted acid sites, associated to polymeric niobium oxide species. Moreover, the stability of catalysts was due to the neutralization of Lewis acid sites of zirconia, which were unselective coke initiator sites.

Omata et al. [21] also synthesized W–Nb mixed oxides with a layered structure in the *c*-direction, prepared under hydrothermal conditions and calcined between 400 to 1000 °C. The W–Nb–O catalysts calcined at lower temperature resulted in a high acrolein yield (>70%). The temperature of calcination influenced on the structure of the *a*–*b* plane, affecting to the product distribution. However, W–Nb–O catalysts calcined at 1000 °C, with an ordered arrangement based on the $Nb_8W_9O_{47}$, gave a higher yield of hydroxyacetone and lower of acrolein, whereas the calcination at 700 °C gives rise to a disordered arrangement, and the acrolein yield increased.

In the present study, zirconium doped mesoporous silica has been used as support for the preparation of a new family of niobium based catalysts. The support was prepared following a synthetic route similar to that of SBA-15 materials in order to gain in hydrothermal stability; moreover, the Si/Zr molar ratio was fixed at 5 since, in a previous work [28], it was demonstrated the good catalytic performance of a MCM-41 catalyst with such molar ratio. The niobium loading was varied in a wide range in order to obtain different superficial niobium species and correlate the nature of these species with acid properties and product selectivity in the gas phase dehydration of glycerol.

2. Experimental

2.1. Catalyst preparation

A zirconium doped mesoporous silica was synthesized by using P123 (Poly(ethylene glycol)-block-poly(propylene glycol)-block-poly(ethylene glycol, Aldrich)) as structure directing agent. Firstly, P123 was dissolved in a 1.7 M HCl aqueous solution, under magnetic stirring at 40 °C. Then, silicon and zirconium precursors (tetraethyl orthosilicate (Aldrich) and zirconium *n*-propoxide (Aldrich), respectively) were added dropwise, with a Si/Zr molar ratio of 5. The final molar composition of the synthesis gel was $P123/SiO_2/ZrO_2/HCl/H_2O = 1/55/11/350/11100$. The resulting suspension was stirred at 40 °C for 72 h. The solid product was recovered by filtration, washed with deionized water and dried at 60 °C. Finally, it was calcined in air at 550 °C for 6 h with a heating rate of 1 °C min^{-1}. This support was labeled as SiZr5.

The niobium was supported by incipient wetness impregnation, using niobium oxalate/oxalic acid solutions [50], with nominal values of Nb_2O_5 ranging between 1 and 12 wt%. Solids were dried in an oven at 60 °C, and then calcined at 400 °C during 4 h (heating rate of 2 °C min^{-1}). Niobium catalysts were labeled as *x*Nb where *x* stands for wt% of Nb_2O_5.

2.2. Catalyst characterization

Powder diffraction patterns were collected on an X'Pert ProMPD automated diffractometer equipped with a Ge (1 1 1) primary monochromator (strictly monochromatic Cu-Kα radiation) and a X'Celerator detector.

X-ray photoelectron spectroscopy (XPS) studies were performed with a Physical Electronics PHI 5700 spectrometer equipped with a hemispherical electron analyzer (model 80-365B) and a Mg Kα (1253.6 eV) X-ray source. High-resolution spectra were recorded at 45° take-off-angle by a concentric hemispherical analyzer, operating in the constant pass energy mode at 29.35 eV, using a 720 μm diameter analysis area. Charge referencing was done against adventitious carbon (C 1s at 284.8 eV). The pressure in the analysis chamber was kept lower than 5×10^{-6} Pa. PHI ACCESS ESCA-V6.0 F software package was used for data acquisition and analysis. A Shirley-type background was subtracted from the signals. Recorded spectra were always fitted using Gauss–Lorentz curves in order to determine more accurately the binding energy of the different element core levels.

N_2 adsorption–desorption isotherms at −196 °C were obtained using a gas adsorption analyzer from Micromeritics, Inc. (ASAP 2020 model). Prior to N_2 adsorption, samples were evacuated at 200 °C (heating rate 10 °C min^{-1}) for 18 h. Pore size distributions

and pore volume were calculated with the BJH method applied to the adsorption branch of the isotherms.

FT-IR spectra were registered on a Varian 3100 FT-IR spectrophotometer. The interferograms consisted of 200 scans, and the spectra were collected using a KBr spectrum as background. For each spectrum, about 30 mg of finely ground catalyst were placed in the sample holder.

FTIR spectra of adsorbed pyridine were recorded on a Shimadzu 8300 FTIR spectrometer at a resolution of 4 cm^{-1}. Each spectrum was average over 128 scans. Self-supporting wafers of the samples with a weight/surface ratio of about 12 mg cm^{-2} were placed in a vacuum cell with greaseless stopcocks and CaF_2 windows. The samples were evacuated at 350 °C and 10^{-4} Torr overnight, exposed to pyridine vapors for 15 min at room temperature, and then degassed at different temperatures. The net FTIR spectra of adsorbed pyridine were obtained after subtracting the background spectrum of the solid.

Temperature programmed desorption of ammonia (NH_3–TPD) was carried out to evaluate the total surface acidity of the catalysts. 80 mg of catalyst were pre-treated at 400 °C at atmospheric pressure in a helium flow (40 mL min^{-1}) with a heating rate of 10 °C min^{-1}. The catalyst was cooled down to 100 °C and then ammonia adsorption took place. The NH_3–TPD using a helium flow was performed by raising the temperature from 100 to 550 °C at a heating rate of 10 °C min^{-1} followed by an isothermal period at 550 °C for 15 min. The evolved ammonia was analyzed by online gas chromatography (Shimadzu GC-14A) equipped with a TCD. In order to quantify the amount of desorbed ammonia, the equipment was previously calibrated by measuring the corresponding signals of known amounts of pure ammonia.

Raman spectra were obtained by using a Raman Senterra (Bruker) microspectrometer equipped with a thermoelectrically cooled charge coupled device (CCD) detector. A Nd:YAG laser was used as the excitation source at 1064 nm and the laser power was set to 100 mW, the spectral resolution was of 4 cm^{-1} and each spectrum is averaged from 7000 accumulations. Raman spectra were performed on powder samples without any previous treatment.

2.3. Catalytic study

The dehydration of glycerol was performed in an atmospheric-pressure fixed-bed continuous-flow stainless steel catalytic reactor (9.1 mm in diameter, and 230 mm in length), operated in the down-flow mode. The reaction temperature was measured with an interior placed thermocouple in direct contact with the catalyst bed. For the activity tests, 0.5 g of catalyst (particle size 0.85–1.00 mm) diluted with SiC to 3 cm^3 volume was used. Prior to the catalytic test, catalysts were pre-treated in situ at atmospheric pressure under a N_2 flow of 30 mL min^{-1}, at 325 °C for 0.5 h. The glycerol aqueous solution (10 wt%) was supplied by means of a Gilson 307SC piston pump (model 10SC) at 0.1 ml min^{-1} feed rate under a N_2 flow (15 mL min^{-1}). The evolution of catalytic tests was studied by collecting liquid samples after different time-on-stream (TOS) values, in a vial cooled with an ice trap. The collected liquid was analyzed by gas chromatography (Shimadzu GC-14B, equipped with a flame ionization detector and a TRB-14 capillary column).

The glycerol conversion (mol%) and the selectivity to the identified and calibrated products have been calculated as follows:

$$C\,(\%) = \frac{n_{\mathrm{Gly,in}} - n_{\mathrm{Gly,out}}}{n_{\mathrm{Gly,in}}} \times 100$$

$$S_i\,(\%) = \frac{n_i}{n_{\mathrm{Gly,in}} - n_{\mathrm{Gly,out}}} \times \frac{z_i}{z_{\mathrm{Gly}}} \times 100$$

$$y_i\,(\%) = \frac{C \times S_i}{100}$$

where n_{in} and n_{out} represent the mol of glycerol at the inlet and outlet of the reactor. n_i is the molar concentration of the product i at the outlet of the reactor and z_i and z_{Gly} are the number of atoms of carbon of the product i and glycerol respectively. The carbon balance (mol%) was calculated by summing up the unreacted glycerol and the total quantities of detected and calibrated products.

3. Results and discussion

3.1. Characterization of catalysts

The aim of the present work was to study the catalytic performance of a family of niobium supported catalysts in the dehydration of glycerol to acrolein. For this purpose, a mesoporous silica–zirconia mixed oxide was synthesized as support and the niobium species were deposited on its surface by means of incipient wetness impregnation.

The mesoporous character of the support was confirmed from XRD analysis and the nitrogen adsorption–desorption isotherms. Thus, at low diffraction angle, a broad peak centered at $2\theta = 2.15°$, resulting from the arrangement of mesoporous channels with a periodic distance of 4.1 nm, can be observed (Fig. 1S, Supplementary information) [51,52]. At high angles, the absence of diffraction peaks attributable to crystalline zirconia and silica reveals the amorphous nature of the pore walls (Fig. 2S, Supplementary information). The peak at low angle is maintained after the niobium species were supported, confirming the stability of the mesoporous structure. Moreover, diffraction peaks of niobium species are not detected, even for the highest niobium loading.

The N_2 isotherms of Type IV, according to the IUPAC classification, with a hysteresis loop closing at P/P_0 of 0.42, confirm the mesoporous nature of the support and niobium catalysts [52], although with a broad range of pore sizes, as can be inferred from the absence of a steep nitrogen condensation in a narrow range of relative pressures (Fig. 1a). This feature was confirmed by the pore size distribution, which shows the existence of pores ranging between 1.7 to 6 nm (Fig. 1b). The presence of niobium species, mainly for loadings higher than 8 wt%, provokes a decrease of BET surface area, total pore and micropore volumes (Table 1).

The FTIR spectra (Fig. 2a) exhibit the skeletal vibrations of the siliceous framework in the wavenumber region between 500 and 1300 cm^{-1}. Thus, the asymmetric stretching mode of the Si—O—Si bond appears at 1055 cm^{-1} [53–55], and a shoulder at 1130 cm^{-1}, which is downshifted respect to silica (*ca.* 1100 cm^{-1}) [56], may be-attributed to Si—O—Zr groups [57]. On the other hand, the band at 800 cm^{-1} can be associated to the symmetric stretching mode of Si—O—Si groups [54,58,59]. Finally, the formation of segregated ZrO_2 could be ruled out since a characteristic band of ZrO_2 at 735 cm^{-1} is not observed [56].

After supporting niobium oxide, some discernible features associated to niobium species can be detected. Thus, the intensity and complexity of the band centered about 970 cm^{-1} is increased when niobium species are present. This band is characteristic of Nb=O vibrations of monooxoniobate species [60–62]. In addition, as niobia loading is increased up to 12 wt%, a new band arises at 930 cm^{-1}, which could be assigned to the stretching modes of Nb—O—Nb bonds in polymerized NbO_x species [61]. Moreover, a new weak band at 750 cm^{-1}, observed for niobia loading higher than 8 wt%, could be ascribed to chain Nb—O—Nb linkages [62]. Therefore, the presence of bands at 930 and 750 cm^{-1} could point out the formation of polymerized NbO_x species, which are not detected by XRD due to its small size or amorphous character.

Table 1
Textural parameters and total acidity of SiZr5 support and *x*Nb catalysts.

Catalyst	S_{BET} ($m^2\ g^{-1}$)	*t*-plot ($m^2\ g^{-1}$)	V_p ($cm^3\ g^{-1}$)	d_p (Å)	μmol[a] $NH_3\ g^{-1}$	μmol[b] $NH_3\ m^{-2}$	At[c] Nb nm^{-2}	B/L[d]
SiZr5	812	131	0.395	33	477	0.59	–	0.65
1Nb	656	282	0.228	31	354	0.54	0.17	0.64
4Nb	578	213	0.266	31	590	1.02	0.70	0.76
8Nb	556	156	0.281	36	669	1.2	1.39	1.36
12Nb	496	120	0.248	38	600	1.21	2.09	1.11
8Nb_R[e]	432	144	0.234	39	472	1.09	1.39	0.35

[a] Total acidity calculated by means of NH_3–TPD.
[b] Intrinsic acidity.
[c] Surface atomic concentration of Niobium per nm^2.
[d] Ratio of the concentration of Brönsted and Lewis acid sites calculated from the adsorption of pyridine evacuated at 100 °C.
[e] 8Nb catalyst regenerated in a flow of air at 550 °C during 4 h.

The FTIR technique also renders information about the condensation of niobium species with the surface hydroxyl groups of the support, following the evolution of the OH stretching mode in the region of 2600–4000 cm^{-1}. As shown in Fig. 2b, the support shows a sharp band at 3745 cm^{-1} associated to isolated silanol groups, together with a broad band extending up to 2800 cm^{-1} due to the existence of hydrogen bond between water molecules and silanol groups [59]. Niobium catalysts display similar features, even for high niobia content, indicating that the monolayer coverage is not achieved even with 12 wt% of niobium oxide. This is a consequence of the low number and reactivity of the surface hydroxyl groups [63,64] due to the covalent character of SiO_2, resulting in a poor dispersion of active phases based on metal oxides [48]. Thus, Massa et al. [48] have reported, based on FTIR analysis in the OH region, that silanol groups did not react entirely with niobium.

Raman spectroscopy has corroborated the conclusions obtained from FTIR spectra about the identification of both superficial and crystalline niobium oxide species [64]. Firstly, the absence of the characteristic band associated to ZrO_2 particles at 756 cm^{-1} allows excluding its segregation from the zirconium-doped silica walls (Fig. 3) [20,65]. Concerning vibration bands ascribed to niobium species, the existence of bulk niobium oxide (amorphous) could

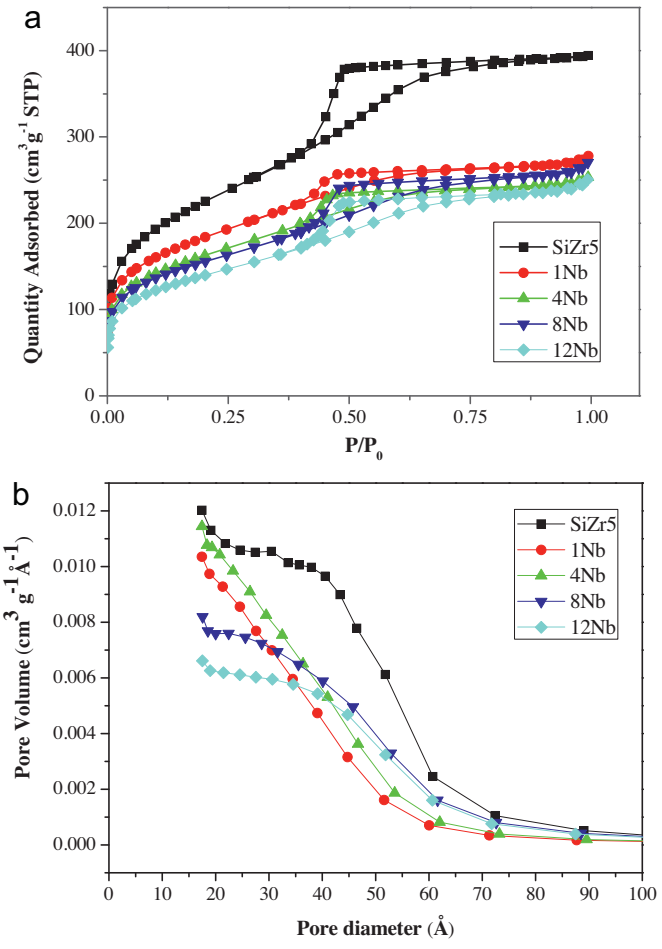

Fig. 1. (a) Nitrogen adsorption isotherms of the SiZr5 support and *x*Nb catalysts; (b) pore size distributions of SiZr5 support and *x*Nb catalysts.

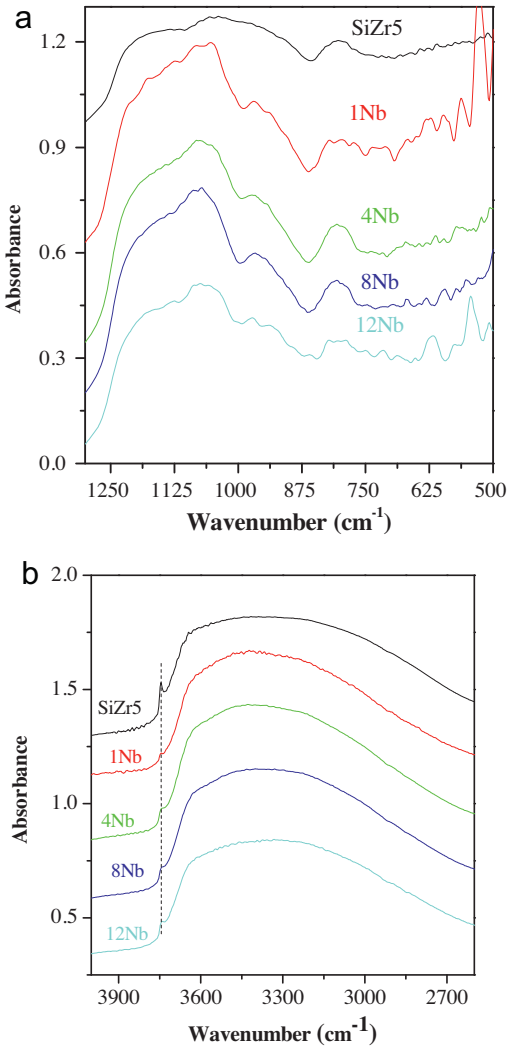

Fig. 2. (a) FTIR analysis of the SiZr5 support and *x*Nb catalysts in the range 500–1200 cm^{-1} and (b) in the range 2600–4000 cm^{-1}.

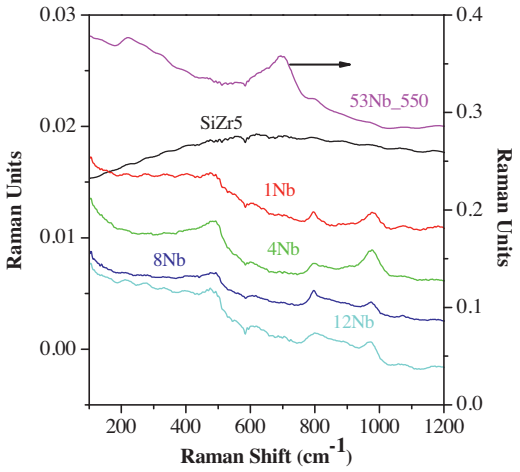

Fig. 3. Raman spectra recorded under ambient conditions of the support and *x*Nb catalysts. For comparison, it is included the Raman spectra of a sample with 53 wt% Nb_2O_5.

be also discarded due to the absence of the band at ~690 cm^{-1} [20,64,66,67]. It has been previously reported that crystalline niobia is detected when the coverage exceeds the monolayer and the calcination temperature is higher than 400 °C [65]. In this sense, a sample with 53 wt% Nb_2O_5 loading was prepared and calcined at 550 °C (53Nb_550) to prove this assumption. Its Raman spectrum shows bands at 700 and 200 cm^{-1}, emerging from the presence of bulk niobium oxide [65,68]. Niobium catalysts exhibit a band at ~975 cm^{-1} which has been previously assigned to the Nb=O vibration mode of surface NbO_4 species [65,69]. This band is asymmetric and broad, which could indicate the existence of different types of Nb=O species. This behavior is similar to that reported by Onfroy et al. and Xia et al. [60,70] for niobium supported on TiO_2 and ZrO_2, who assigned this band to the existence of various Nb surface species, exhibiting different degree of condensation. At 830 cm^{-1}, it appears a band already observed for 4Nb catalyst which is broaden with niobium loading and is attributed to the vibration of the Nb—O—Nb linkages of oligomeric species [70,71]. Another broad band is observed at 900 cm^{-1} which was assigned to the Nb—O—Si bond [69].

XPS study allows getting insights into the superficial composition and chemical environment of elements present on the surface of catalysts (Table 2). Thus, the photoelectronic peak of the O 1s core level is asymmetric and can be deconvoluted into two contributions: 530.6–531.1 and 532.8–532.9 eV. The former BE value is higher than that reported for ZrO_2 (529.9–530.2 eV) [72–75], again discarding the presence of segregated ZrO_2, which is corroborated by considering the Zr 3d core level at 183.2 eV (0.9–1 eV higher than the value reported for ZrO_2 [72–75]), attributed to Si—O—Zr bonds. The higher BE contribution of the O 1s is more intense and agrees quite well with values found in the literature for O 1s in SiO_2 (533 eV) [57,73–76]. However, Pietre et al. [77] studied the niobic acid and found that O 1s core level was the sum of two different contributions: 532.3 eV and 530.4 eV, which were attributed to oxygen in Nb=O and Nb—OH, respectively [75–77]. In this sense, for the niobium containing catalysts, the signals associated to these types of oxygen could overlap with the two contributions already proposed for the support, since there is not a clear correlation between the niobium loading and the intensity of both contributions.

The Nb 3d core level is formed by the $3d_{5/2}$ (*ca.* 207.8 eV) and $3d_{3/2}$ (*ca.* 210.6 eV) doublet, with a spectral separation of 2.8 eV. These values are typical of Nb(V) [48,78] and barely vary regardless of niobium loading, without the presence of reduced Nb(IV) species (206.5 eV) [48]. This doublet is hardly distinguished for catalysts

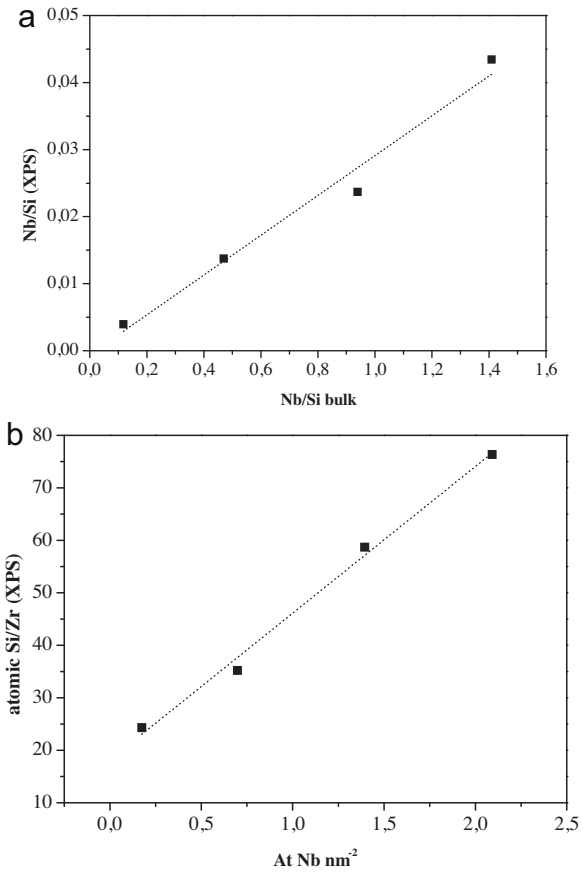

Fig. 4. (a) Variation of Nb/Si atomic ratio with the bulk Nb/Si ratio and (b) variation of Si/Zr atomic ratio with increasing the Nb surface density.

with a niobia loading lower than 8 wt% (Fig. 3S, Supplementary information), where a very broad band is observed due to the high dispersion of niobium species onto the support surface [79].

Regarding the superficial Nb/Si atomic ratio (Fig. 4a), there is a linear relationship between superficial and bulk Nb/Si atomic ratios, which clearly points out a suitable dispersion of NbO_x species (isolated and bidimensional structures) on the support surface, without formation of tridimensional particles of niobium oxide [68]. Therefore, the preparation of these Nb-containing catalysts has led to a high dispersion of niobium oxide, which demonstrates the positive effect of zirconium. In this sense, Jehng et al. [67,68] suggested that the monolayer of niobium was accomplished with 2 wt% Nb_2O_5 when SiO_2 (275 m^2/g) was used as support, whereas our results show that the monolayer is not achieved even for the catalyst with 12 wt% Nb_2O_5. The lower capacity of silica to achieve higher surface coverage has been attributed to the lower density and reactivity of hydroxyls groups relative to other oxidic supports [64]. Nevertheless, the surface Nb/Si atomic ratios are much lower than the corresponding bulk ratios, which could be explained by the preferential location of Nb into the porous network, thus rendering difficult its detection by XPS. Fig. 4b shows that the surface Si/Zr atomic ratio is increased with the niobium loading; this effect could point out that niobium species are mainly located on zirconium domains, perhaps due to the tendency of Zr species to increase their coordination by interaction with oxygen of niobium species.

The number and strength of the acid centers were evaluated by means of NH_3–TPD. The total concentration of acid sites per gram of catalyst is collected in Table 1 and the NH_3–TPD curves are depicted in Fig. 6S (Supplementary information). The support exhibits a significant amount of acid centers, being the zirconium

Table 2
Surface characterization of SiZr5 support and *x*Nb catalysts determined by XPS analysis.

Catalyst	Si 2p (eV)	Zr $3d_{5/2}$ (eV)	O1s (eV)		Nb $3d_{5/2}$ (eV)	Superficial atomic ratio	
						Si/Zr	Nb/Si
SiZr5	103.3	183.2	530.7 (2.20%)	532.8 (97.7%)	–	36.05	–
1Nb	103.4	182.9	530.6 (4.70%)	532.9 (95.3%)	207.8	24.29	0.004
4Nb	103.4	183.2	531.1 (6.80%)	532.9 (93.2%)	207.7	35.20	0.014
8Nb	103.3	183.0	531 (4.40%)	532.8 (95.60%)	207.8	58.67	0.024
12Nb	103.3	182.9	530.8 (5.50%)	532.8 (94.50%)	207.4	76.34	0.043

the responsible of them. The acid sites are mainly associated to the presence of superficial Zr(IV) species with low coordination into the mesoporous network [80].

NH_3–TPD curves of supported niobium catalysts are also broad and extend to 550 °C, evidencing a heterogeneous distribution of acid strengths. It is noticeable that the strength of acid sites seems to increase with the niobium loading up to 4 wt% Nb_2O_5, then slightly decreases for the 8Nb catalyst (Fig. 4S, Supplementary information) and finally the shape of 12Nb catalyst curve resembles to both SiZr5 and 1Nb catalyst. Among the niobium catalysts, the 4Nb exhibits the highest proportion of strong acid sites. The number of acid sites increases with the niobium loading, except the 1Nb catalyst which shows a lower acidity than the support (Table 1). In fact, the TPD curves of both support and 1Nb catalyst are quite similar, mainly differing in the intensity of the maximum at low temperature. Ladera et al. [81] and Lauriol-Garbey et al. [36] observed a decrease in the amount of acid centers when niobium oxide was supported on TiO_2 and ZrO_2, respectively. The rest of catalysts showed a higher concentration of acid sites, but the highest density of acid sites is reached for the 8Nb and 12Nb catalysts. Therefore, niobium loading higher than 8 wt% does not lead to an increase in the intrinsic acidity of catalysts.

The nature of acid sites, i.e. Brönsted or Lewis acid character, can be followed by means of pyridine adsorption coupled to FTIR analysis (Fig. 5S, Supplementary information). The support and niobium catalysts exhibit the same spectral features, ascribed to C—C vibrations of the pyridine skeleton after its adsorption on the catalyst surface. The bands appearing between 1400 and 1700 cm^{-1} correspond to the 8a (*ca.* 1608 cm^{-1}) and 19b (*ca.* 1447 cm^{-1}) mode vibrations of pyridine coordinated on Lewis acid centers (LAS), and the 8a (*ca.* 1637 cm^{-1}) and 19b (*ca.* 1542 cm^{-1}) to pyridine adsorbed on Brönsted acid sites (BAS) [82–84]. There is also a band at *ca.* 1597 cm^{-1}, which can be assigned to the 8a mode vibration of pyridine bonded by hydrogen bond to the catalyst surface through superficial hydroxyls. The intense band at 1491 cm^{-1} corresponds to the 19a mode vibration of the pyridine associated both Brönsted and Lewis acid sites. Similarly to the SiZr5 support [80], the niobium catalysts exhibit both types of acid sites.

According to the NH_3–TPD data, the 1Nb catalyst exhibits a concentration of both BAS and LAS lower than that of SiZr5 (Table 1S, Supplementary information). In this sense, supporting niobium oxide on the support neutralizes the most active hydroxyl groups, thus decreasing the amount of BAS, and the covering of LAS of the support could be substituted by other LAS associated to Nb species, mainly isolated NbO_4 groups, very dispersed on the surface, causing a lower concentration of superficial niobium species. However, regarding the LAS concentration, the 4Nb catalyst shows the highest concentration, although an increase of niobium loading has a negative effect, provoking a decrease of the concentration. When the niobium loading is increased from 1 to 4 wt%, the concentration of isolated NbO_4 groups is also raised, and therefore also the amount of LAS. This fact is supported by the Raman analysis (Fig. 4), which reveals that the band at 975 cm^{-1} increases its intensity with the metallic loading. As it was mentioned before, this band is related to the monooxoniobates Nb═O which are responsible of the LAS. For 8Nb and 12Nb catalysts, the intensity of this band decreased and concomitantly the concentration of LAS. Therefore, the 4Nb catalyst presents the highest LAS concentration and the 8Nb catalyst shows the highest amount of BAS.

On the other hand, the BAS concentration is increased at 100 °C with the niobium loading (Fig. 5S, Supplementary information) up to 8 wt% of niobium oxide and decrease with further niobium loading. Datka et al. [83] and Xia et al. [70] have found, studying supported niobium catalysts, that the BAS arise from certain niobium loading, at which the polymeric species NbO_x are present and favored the formation of such acid centers. Therefore, in this case, the highest BAS concentration is achieved when the niobium loading is comprised between 4 and 8 wt%. In this niobium loading range, niobium species would grow as bi-dimensional structures whereas higher niobium loading would lead to the formation of 3-dimensional Nb_2O_5 species. For example, Onfroy et al. and Xia et al. [60,70] observed that isopropanol conversion to propylene was dependent on the concentration of Brönsted acid sites, and these BAS were associated to the existence of polymeric NbO_x species.

The study of pyridine desorption, after evacuation at different temperatures, has demonstrated that BAS are stronger than LAS, although the intensity of bands associated to both types of acid sites decreases at higher temperatures (Fig. 5S, Supplementary information). Thus, the band at 1596 cm^{-1} is largely reduced after thermal treatment at 100 °C, evidencing the weak interaction of pyridine with surface hydroxyl groups.

On the other hand, the spectra of niobium catalysts show intense bands at 1680 and 1558 cm^{-1}, whose intensities are increased with the evacuation temperature and decrease with the niobium loading. The FTIR spectrum also evidences these bands, but less intense, which have been ascribed to the reaction of pyridine with the catalyst surface [33,85–87]. This process takes place by a nucleophilic attack of hydroxyl groups to a pyridine molecule coordinated on a Lewis acid site. It is noteworthy that these bands are present even at 25 °C, when, in other studies, they appear at temperatures as high as 300 °C [85,86]. These stronger acid centers could be associated to Nb═O bond of tetrahedral niobia [88]. Moreover, taking into account the low temperature of this reaction, it could be thought that the nucleophilic hydroxyl group should be located near to this pyridine molecule activated on LAS, and thereforethis OH group could be bonded to niobium (Scheme 1, Supplementary information).

In summary, it could be inferred from data extracted from these different characterization techniques that the nature of Nb species depends on the niobium loading. Thus, Nb_2O_5 loading lower than 1 wt% lead to the formation of isolated tetrahedral NbO_4 species anchored to the catalyst surface by a variable number of

Table 3
Catalytic performance in the reaction of glycerol of SiZr5 support and *x*Nb catalysts at 2 h and 8 h of time on stream.

Catalyst	Conversion (%)	Product selectivity (%)				Acrolein yield (%)	C balance (%)
		Acrolein	Acetaldehyde	Hydroxyacetone	Others		
SiZr5	91	25	22	5	49	22	55
	(72)	(23)	(20)	(7)	(50)	(17)	(64)
1Nb	77	27	19	6	48	21	63
	(59)	(24)	(14)	(5)	(57)	(14)	(67)
4Nb	86	35	14	7	45	30	62
	(55)	(30)	(10)	(6)	(55)	(16)	(70)
8Nb	77	45	13	10	32	35	75
	(45)	(45)	(11)	(8)	(36)	(20)	(84)
12Nb	79	33	9	7	51	26	60
	(55)	(35)	(8)	(8)	(49)	(19)	(73)

Experimental conditions: weight of catalys = 0.5 g diluted with SiC to 3 cm^3 volume. Feed composition: 10 wt% glycerol in water; liquid flow = 0.1 mL min^{-1}; N_2 flow = 15 mL min^{-1}; T = 325 °C. In brackets TOS at 8 h.

Nb—O—Si(Zr) linkages. These species are associated to both Lewis and Brönsted acid sites depending on the number of such bonds (Scheme 1a, Supplementary information). This type of niobium species have been also proposed by Burke and Ko [62], Pittman and Bell [71] and Yoshida et al. [89]. The amount of these isolated tetrahedral species increases with the Nb_2O_5 content, as supported by the higher intensity of the Raman band at 976 cm^{-1}, and the polymerization takes place (Raman band at 830 cm^{-1}) as the niobia loading increases. In this sense, the 8Nb catalyst evidences the existence of polymeric NbO_x species causing a 2D growing of the niobium oxide (Scheme 1b, Supplementary information) and, on the other hand, the isolated tetrahedral species are not as prevalent. Finally, from the characterization of *x*Nb catalysts, it could be deduced that the dispersion of niobium species is very high even for the highest niobium loading. However, the 12Nb catalyst showed neither an increase of acidity (Table 1) nor an increase of the Brönsted acid sites concentration, which could point out that some structural changes occur when the niobium loading is increased up to 12 wt%. Thus, a transition between tetrahedral niobium species, found at low niobium loadings, to octahedrally coordinated ones could take place. As the Brönsted acid sites amount decreases more markedly than Lewis acid sites (Table 1S), it could be postulated that these octahedral species are highly distorted NbO_6, as claimed by Datka et al. [83], Jehng and Wachs [65] and Burke and Ko [62] for Nb/SiO_2 catalysts.

3.2. Catalytic performance

This series of supported niobium catalysts has been tested in the dehydration of glycerol, at atmospheric pressure, in gas phase at 325 °C, feeding to the catalytic bed a 10 wt% of glycerol aqueous solution, with a WHSV of glycerol of 1.3 h^{-1}, corresponding to a contact time of 12 s.

Under these experimental conditions, the main detected products were acrolein, acetaldehyde and hydroxyacetone. The catalytic performance of niobium-based catalyst and the SiZr5 support is gathered in Table 3 and depicted in Fig. 6S (Supplementary information). Under the label "Others" are included all those not analyzed products.

The catalytic dehydration of glycerol requires water-tolerant catalysts due to the presence of high amounts of water during reaction. Therefore, the development of water-resistant catalysts is essential, and, in this sense, niobium catalysts have shown to be stable in different catalytic processes, such as dehydration of monosaccharides and oligosaccharides from biomass [90–93], esterification of fatty acids and transesterification of triglycerides [77,94,95].

Firstly, it is worthy to point out that silica is not active in this reaction [28,33,48] due to the lack of acid centers, but the incorporation of zirconium provides acid properties, as previously reported [80]. This is corroborated by the noticeable catalytic activity of the SiZr5 support, which attains a glycerol conversion of 91 mol% after 2 h of reaction, and its stability with TOS, 72 mol% after 8 h. However, the support is not very selective toward the formation of acrolein (Table 3), since selectivities to acrolein and acetaldehyde, after 2 h of TOS, are 25 and 22 mol%, respectively. Furthermore, the carbon balance is very poor, with a value of 64% after 8 h of TOS, pointing to the formation of carbonaceous deposits on the catalyst surface. On the other hand, supported niobium catalysts show high conversion of glycerol, although lower than that of the support (Fig. 6S, Supplementary information). Among them, the 4Nb catalyst is the most active, achieving a glycerol conversion of 86 mol% after 2 h, and maintaining a value of 55 mol% after 8 h. On the other hand, the 8Nb catalyst displays the lowest glycerol conversion (45 mol%) after 8 h. This decay of glycerol conversion with TOS has been previously reported in the literature for niobium catalysts supported on zirconia [20] and silica [47], although niobium loadings and the catalytic conditions were different from those used in the present work. These catalytic results do not improve those reported by Lauriol-Garbey et al. [32,46] whose attained a glycerol conversion of 82% during 177 h, maintaining an acrolein selectivity of 72%. However, our results are similar to those obtained with a silica supported niobium catalyst [47]. These authors obtained glycerol conversion of over 70% at the early stages of reaction. Massa et al. [48] also reported a catalyst based on niobium supported on ZrO_2 showing a nearly complete glycerol conversion and acrolein selectivity of 75% after 3 h. Nevertheless, it must be emphasized that a more accurate comparison of the different families of catalysts should be inferred by using similar experimental conditions in the gas-phase dehydration of glycerol; otherwise, it is very difficult to draw precise conclusions.

On the other hand, the catalytic behavior of the 8Nb catalyst was compared with a catalyst with the same niobia content, but supported on a mesoporous silica without zirconium. The catalytic data evidence a lower glycerol conversion and acrolein yield (63.1 and 23.3 mol%, respectively, after 2 h of TOS), under similar experimental conditions, in the absence of zirconium. Thus, the presence of zirconium ameliorates the glycerol conversion and acrolein yield, being probably due to the lower total acidity of 8Nb-Si (277 μmol NH3 g^{-1}) in comparison with the 8Nb–SiZr catalyst (669 μmol NH3 g^{-1}).

Nevertheless, clear relationships between total acidity, as measured by means of NH_3–TPD, and stability with TOS neither the intrinsic acidity (μmol desorbed NH_3 m^{-2}) and glycerol conversion can be deduced. However, it could be inferred from NH_3–TPD curves (Fig. 4S, Supplementary information) that catalysts with a lower amount of strong acid sites are most stable. These results agree with those reported by Lauriol-Garbey et al. [32] and Massa

et al. [20], although Suprun et al. [96] found that high acid sites density is necessary for attaining high initial glycerol conversion. Also, in this sense, the external surface area seems to play an important role to delay the catalyst deactivation, since the SiZr5 support shows higher external surface and hence higher stability with TOS. The influence of textural parameters over the catalytic performance was evaluated by Tsukuda et al. [15], who observed that a suitable pore size is required to attain the highest glycerol conversion and acrolein selectivity. Moreover, Yun et al. [27] demonstrated that a hierarchical-pore structured acid functionalized silica catalyst was stable and highly selective to acrolein, compared to a microporous HZSM-5 zeolite, since it was very resistant to pore blocking by coke deposition.

On the other hand, in spite of the glycerol conversion is not improved when the niobium oxide is supported, compared with the SiZr5 support, the selectivity toward acrolein is markedly increased (Fig. 7S, Supplementary information). Thus, the selectivity values for the 1Nb and 8Nb catalysts, after 2 h of TOS, are 27 and 45 mol%, respectively. This value is maintained after 8 h of TOS (45 mol%), despite the decrease of glycerol conversion. The stability of acrolein selectivity with TOS has been already reported by others authors using different catalytic systems, such as ZrO_2-supported Nb and W [20], SiO_2-supported Nb [47], MCM-22 zeolite [35] and NbZr mixed oxides [36]. Moreover, the selectivity toward acrolein or hydroxyacetone seems to depend on the type of acid site involved in the dehydration reaction [48]. In this sense, acrolein and hydroxyacetone formation is favored in the presence of Brönsted and Lewis acid sites, respectively [97,98]. Fig. 5a displays the variation of acrolein selectivity and the B/L ratio as a function of the niobium loading. The acrolein selectivity is steadily increased with the niobium loading up to 1.4 at Nb nm^{-2}, which corresponds to 8 wt% Nb_2O_5 and then decreased with further increasing. The B/L ratio follows a similar trend, pointing out that the most selective catalyst is that which possesses the highest B/L ratio, thus demonstrating a clear relationship between Brönsted acid sites and acrolein selectivity.

However, hydroxyacetone does not show the same trend when it is compared with the L/B ratio (Fig. 5b). On the contrary, it is observed an increase of hydroxyacetone selectivity for lower L/B ratios. This fact is opposite to that reported in the bibliography so far [29,48]. Although some papers have stated that hydroxyacetone may be formed on basic sites [25,87], the present niobium based catalysts do not shown any measurable basic sites, neither by means of CO_2–TPD nor by CO_2 adsorption coupled to FTIR analysis, thus discarding the presence of basic sites. Recently, Foo et al. [99] have demonstrated, by using FTIR spectroscopy, the cooperative role of Brönsted and Lewis acid sites in the glycerol dehydration to hydroxyacetone over niobia catalysts. These authors have proposed that this reaction occurs in several steps. Firstly, after glycerol chemisorption, a primary hydroxyl group of glycerol dissociates to form a bridging alkoxy bond (supported by DFT analysis [100]) with two unsaturated metal atoms, while the other primary alcohol group is interacting non-dissociatively with a metal atom. The secondary alcohol may form a hydrogen bond with a surface oxygen atom. Interestingly, these alkoxy bonds are resistant to high temperatures and water vapor [99]. In the second step, the chemisorbed glycerol is transformed into 2-propene-1,2-diol, which further tautomerizes to hydroxyacetone. The authors concluded that the second step involved the participation of an adjacent Brönsted acid site to generate the 2-propene-1,2-diol, because the neutralization of Brönsted acid sites by Na^+ disfavored the enol formation and hence the hydroxyacetone yield. This cooperative mechanism between Lewis and Brönsted acid sites could be the responsible for the increase of hydroxyacetone selectivity with the niobium loading, in such a way that the 8Nb catalyst with the highest B/L ratio also exhibits the highest selectivity to hydroxyacetone. Moreover, glycerol chemisorption can take place on strong Lewis acid sites [99,101], whose presence in niobium catalysts has been inferred from pyridine adsorption coupled to FTIR spectroscopy (Fig. 5S, Supplementary information).

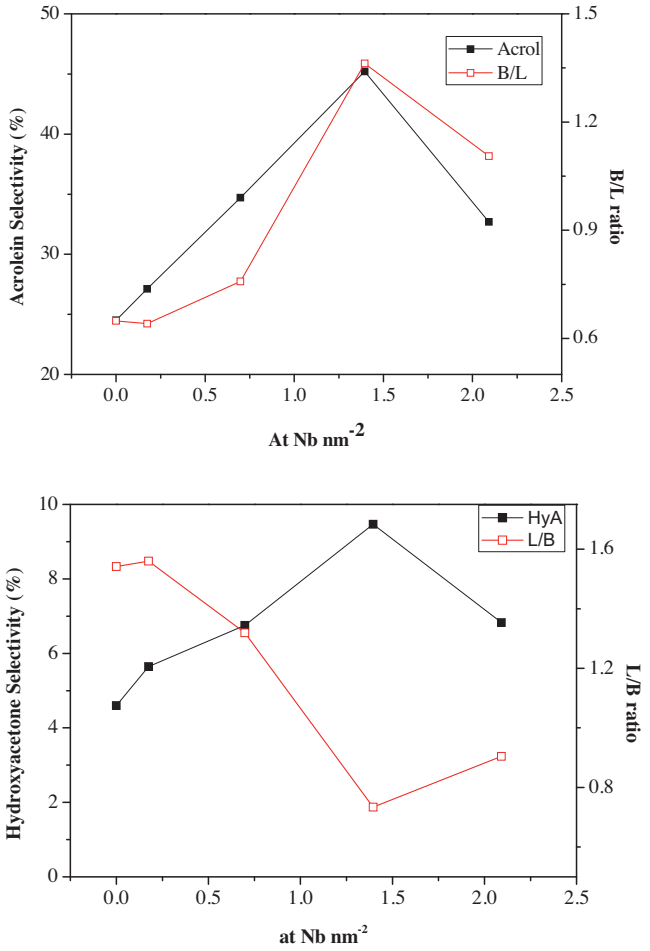

Fig. 5. (a) Dependence of acrolein selectivity and B/L ratio and (b) hydroxyacetone selectivity and L/B ratio, as a function of Nb surface density.

Besides acrolein, acetaldehyde was the most important detected product, but the selectivity to acetaldehyde (Table 3) was decreased as the niobium loading was further increased until 12 wt% Nb_2O_5. A likely route of acetaldehyde formation arises from the decomposition of 3-hydroxypropanal. Yun et al. [27] have proposed that those catalysts in which the regeneration of Brönsted acid sites is not accomplished after the formation of 3-hydroxypropanal, instead of being adsorbed on the catalyst surface; and hence, continuing its dehydration to acrolein, the 3-hydroxypropanal undergoes a homogenous decomposition to acetaldehyde and formaldehyde. Moreover, it has been also proved that the homogeneous decomposition is thermodynamically favored. Thus, Laíno et al. [102] and Nimlos et al. [103] have shown that the energetic barrier of the homogeneous decomposition of 3-hydroxypropanal to acetaldehyde and formaldehyde is lower than the corresponding to acrolein. Therefore, the decrease of acetaldehyde selectivity agrees with this proposed mechanism, since the 8Nb catalyst would exhibit a readily regeneration of Brönsted acid sites, yielding lower acetaldehyde production and improving the acrolein yield. Also, the 8Nb catalyst displays the best carbon balance associated to its lower acetaldehyde selectivity, because both acetaldehyde and formaldehyde have been described as probable intermediates in secondary reactions leading to coke formation [10,96,104].

Therefore, it can be concluded that glycerol conversion depends on the strength of acid sites and textural parameters, whereas the nature of acid sites affects to the selectivity toward the different reaction products. The present family of niobium catalysts show an increase of acrolein selectivity as the B/L ratio is increased. Moreover, the B/L ratio influences on the hydroxyacetone and acetaldehyde selectivity, increasing and decreasing, respectively, their selectivity with the increase of the B/L ratio.

It has been demonstrated that niobium loading affects to the textural and acid properties of catalysts: the total amount, relative strength and nature of acid sites. The nature of niobium species existent on the catalyst surface depends on the Nb_2O_5 loading. In this sense, tetrahedral NbO_4 species are predominant for both 1Nb and 4Nb catalysts to which provides a Lewis acid character. For increasing amount of niobia (8 wt%), oligomeric NbO_x species grow, which is related to an increment of Brönsted acidity. These species could undergo hydrolysis of the Nb—O—Nb bonds [71], appearing new Brönsted acid sites associated to Nb–OH groups. A further increase of niobium led to the formation of amorphous Nb_2O_5 particles, with a concomitant decrease of the amount of Brönsted acid sites. Pittmann and Bell [71], from Raman studies, have reported that Nb—O—Nb linkages are sensitive to the presence of water, as it could be inferred from the disappearance of the associated Raman band if Raman spectrum was recorded in the presence of water. However, this band was recovered when the sample was dehydrated. This mechanism of hydrolysis of the Nb – O – Nb linkages might be operating with the 8Nb catalyst, thus generating new Brönsted acid sites, selective to acrolein. On the other hand, the 8Nb catalyst shows the lower stability with TOS, which could be related to the formation of new Brönsted acid sites by hydrolysis.

Regardless of niobium loading, all catalysts exhibit a significant deactivation with TOS, which could be more related to the acid strength instead of the number and nature of acid sites. Thus, both 4Nb and 8Nb catalysts show the highest ratio of strong acid sites (Fig. 4S, Supplementary information) and therefore, they are deactivated more severely than 1Nb and 12Nb catalysts.

3.3. Catalyst reutilization

With the aim of gaining a comprehensive insight into the deactivation process, the spent 8Nb catalyst (8Nb_S) was characterized. It can be observed in Table 2S that the catalytic process is detrimental to the textural parameters, due to the formation of carbonaceous deposits blocking the porous framework of the 8Nb catalyst. These deposits have been studied by CHN, XPS and TG-DTA. The data reveal the existence of carbonaceous depositsmainly on its external surface, as could be inferred from the high percentage of carbon detected by XPS, in comparison with the value obtained from CHN analysis (Table 2S).

On the other hand, neither the Nb/(Si + Zr) atomic ratio nor the binding energy of niobium, as determined by XPS (Table 2S), suffer a noticeable variation after the catalytic test. This fact highlights that the catalytic process do not affect to the superficial composition of the catalyst.

The thermal stability of coke was evaluated by means of TG-DTA (Fig. 8S, Supplementary information). The DTA plot shows a unique exothermic peak extending from 200 to 650 °C, whose shape points out that carbonaceous deposits comprises both aliphatic and aromatic compounds, being those more resistant to combustion [8,105].

After a catalytic run, the 8Nb_S catalyst was regenerated in situ by means of a thermal treatment at 550 °C under an air flow (15 ml min^{-1}) in order to burn the carbonaceous matter. As the DTA analysis shows (Fig. 8S, Supplementary information), this temperature is high enough for coke removing. Then, a second catalytic run was carried out under the same experimental conditions. The thermal treatment was again repeated and a third and last catalytic run was performed.

The glycerol conversion and product selectivity data are modified after the first catalytic run (Table 3S). Thus, in the second and third runs, although glycerol conversion is higher, the selectivity toward acrolein, hydroxyacetone and acetaldehyde decreases.

In order to gain information about this behavior, the acid properties and textural parameters of the 8Nb catalyst were evaluated after the first catalytic run. It is observed that the thermal treatment at 550 °C of the spent catalyst provokes a decline of the total acidity (Table 1), and even the distribution of acid sites changes, with a higher amount of weak acid sites (Fig. 4S, Supplementary information). Moreover, the B/L ratio is decreased up to 0.35 from an initial value of 1.36 (Table 1). On the other hand, textural parameters are also negatively affected, although their influence on the catalytic performance did not seem to be very important, since glycerol conversion is even increased in spite of this modification. Hence, these results should be rather a consequence of the modification of the superficial active species. It has been previously shown that the 8Nb catalyst surface consists basically of NbO_x species, responsible of the existence of Brönsted acid sites. The catalytic tests were carried out in excess of water, which could hydrolyze the Nb—O—Nb bonds [71], generating new Brönsted acid sites and hence increasing the acrolein selectivity. However, when the catalyst is regenerated under a flow of air at 550 °C, a temperature 150 °C higher than that used for the catalyst precursor, instead of regenerating such Nb—OH species, these could be anchored to the catalyst surface generating new tetrahedral Nb species which behave as Lewis acid sites (Scheme 2, Supplementary information). Consequently, the acrolein selectivity decreases and glycerol conversion increases. Yun et al. [27] demonstrated that the regeneration of Brönsted acid sites is a key factor to maintain the sequential dehydration of glycerol to 3-hydroxypropanal (3-HPA) and to acrolein, since 3-HPA may be adsorbed on Brönsted acid sites and suffer its dehydration to acrolein.

From these catalytic and characterization results, and taking into account the nature of acid species present on the surface of fresh and regenerated catalysts, some conclusions can be drawn. Firstly, the Brönsted acid sites are less active than Lewis ones in spite of that the former are more selective to acrolein. Moreover, the Brönsted acid sites are deactivated more rapidly. This behavior could be inferred from the shift of the acid sites distribution toward lower desorption temperatures, as observed in the corresponding NH_3–TPD curves (Fig. 4S, Supplementary information). Thus, Lewis acid sites would be weaker than Brönsted ones and therefore they deactivate in a less extension, so that glycerol conversion is higher and more stable with TOS. Therefore, deactivation could be related to the acid sites strength. Secondly, the increase in stability after the thermal treatment does not translate into an increase of hydroxyacetone selectivity, as might be thought due to the concomitant increase of Lewis acid sites. Conversely, the selectivity to Others increases and the carbon balance declines. Therefore, the Lewis acid sites may be involved in secondary reactions leading to heavy products deposited on the catalyst surface. Finally, the thermal treatment of the 8Nb_S catalyst at 550 °C is not suitable to prevent the modification of the nature of surface niobium species. Thus, Pittman and Bell [71] found that calcination temperatures between 500 and 700 °C can convert surface Nb_2O_5 species to a *T*-Nb_2O_5 phase. It should be noted that the content of C on the surface (Table 2S) is rather high, and therefore the calcination in air of this coke can provoke hot spots on the catalyst surface, leading to temperatures higher than 550 °C. Therefore, it is evident that other regeneration mechanisms should be investigated. A possibility could be a washing step with an organic solvent in order to eliminate a part of the carbonaceous deposits, prior to a calcination step, and avoiding these hot spots.

4. Conclusions

A family of niobium supported catalysts has been synthesized and tested in the gas phase dehydration of glycerol. The acid properties of the catalysts are related to the superficial species of niobium. Thus, the 8Nb catalyst shows the highest B/L molar ratio and acrolein selectivity but the lowest glycerol conversion. It has been proved that the Brönsted acid sites are more rapidly deactivated than Lewis acid sites and the Lewis acid sites conduct the dehydration of glycerol toward products other than acrolein and hydroxyacetone. The 8Nb catalyst was reactivated at 550 °C under air flow, but this thermal treatment led to a modification of the superficial species, and hence the B/L ratio was markedly decreased, and consequently the glycerol conversion is ameliorated along with a decrease of acrolein selectivity.

Acknowledgements

The authors are grateful to financial support from the Spanish Ministry of Economy and Competitiveness (CTQ2012-38204-C03-02 project), Junta de Andalucía (RNM-1565) and FEDER (European Union) funds.

Appendix A. Supplementary data

Supplementary data associated with this article can be found, in the online version, at http://dx.doi.org/10.1016/j.apcatb.2015.05.014

References

[1] J. Juan, D. Kartika, T. Wu, T. Hin, Bioresour. Technol. 102 (2011) 452–460.
[2] S. Chen, S. Lao-Ubol, T. Mochizuki, Y. Abe, M. Toba, Y. Yoshimura, Bioresour. Technol. 157 (2014) 346–350.
[3] H. Lee, Y. Taufiq-Yap, M. Hussein, R. Yunus, Energy 49 (2013) 12–18.
[4] M. Menetrez, Environ. Sci. Technol. 46 (2012) 7073–7085.
[5] G. Maddikeri, A. Pandit, P. Gogate, Ind. Eng. Chem. Res. 51 (2012) 14610–14628.
[6] B. Katryniok, S. Paul, V. Belliere-Baca, P. Rey, F. Dumeignil, Green Chem. 12 (2010) 2079–2098.
[7] C.A.G. Quispe, C.J.R. Coronado, J.A. Carvalho Jr., Renew. Sustain. Energy Rev. 27 (2013) 475–493.
[8] L. Qadariyah, M. Sumarno, S. Machmudah, Wahyudiono, M. Sasaki, M. Goto, Bioresour. Technol. 102 (2011) 9267–9271.
[9] L. Ott, M. Bicker, H. Vogel, Green Chem. 8 (2006) 214–220.
[10] M. Climent, A. Corma, S. Iborra, Green Chem. 16 (2014) 516–547.
[11] Y. Gu, N. Cui, Q. Yu, C. Li, Q. Cui, Appl. Catal. A 429 (2012) 9–16.
[12] L. Possato, R. Diniz, T. Garetto, S. Pulcinelli, C. Santilli, L. Martins, J. Catal. 300 (2013) 102–112.
[13] Z. Wang, L. Wang, Y. Jiang, M. Hunger, J. Huang, ACS Catal. 4 (2014) 1144–1147.
[14] H.P. Decolatti, B.O. Dalla Costa, C.A. Querini, Micropor. Mesopor. Mater. 204 (2015) 180–189.
[15] E. Tsukuda, S. Sato, R. Takahashi, T. Sodesawa, Catal. Commun. 8 (2007) 1349–1353.
[16] B. Katryniok, S. Paul, M. Capron, V. Belliere-Baca, P. Rey, F. Dumeignil, ChemSusChem 5 (2012) 1298–1306.
[17] L. Shen, Y. Feng, H. Yin, A. Wang, L. Yu, T. Jiang, Y. Shen, Z. Wu, J. Ind. Eng. Chem. 17 (2011) 484–492.
[18] M. Haider, C. D'Agostino, N. Dummer, M. Mantle, L. Gladden, D. Knight, D. Willock, D. Morgan, S. Taylor, G. Hutchings, Chem. -Eur. J. 20 (2014) 1743–1752.
[19] L. Liu, B. Wang, Y. Du, A. Borgna, Appl. Catal. A 489 (2015) 32–41.
[20] M. Massa, A. Andersson, E. Finocchio, G. Busca, F. Lenrick, L. Wallenberg, J. Catal. 297 (2013) 93–109.
[21] K. Omata, S. Izumi, T. Murayama, W. Ueda, Catal. Today 201 (2013) 7–11.
[22] S. Chai, B. Yan, L. Tao, Y. Liang, B. Xu, Catal. Today 234 (2014) 215–222.
[23] R. Znaiguia, L. Brandhorst, N. Christin, V. Baca, P. Rey, J. Millet, S. Loridant, Micropor. Mesopor. Mater. 196 (2014) 97–103.
[24] S. Chai, L. Tao, B. Yan, J. Vedrine, B. Xu, Rsc Adv. 4 (2014) 4619–4630.
[25] A. Ulgen, W. Hoelderich, Catal. Lett. 131 (2009) 122–128.
[26] A. Ulgen, W. Hoelderich, Appl. Catal. A-Gen. 400 (2011) 34–38.
[27] D. Yun, T. Kim, D. Park, Y. Yun, J. Han, J. Yi, ChemSusChem 7 (2014) 2193–2201.
[28] C. Garcia-Sancho, R. Moreno-Tost, J. Merida-Robles, J. Santamaria-Gonzalez, A. Jimenez-Lopez, P. Maireles-Torres, Appl. Catal. A 433 (2012) 179–187.
[29] Y. Choi, H. Park, Y.S. Yun, J. Yi, ChemSusChem 8 (2015) 974–979.
[30] G. Srinivasa Rao, N. Pethan Rajan, M. Hari Sekhar, S. Ammaji, K.V.R. Chary, J. Mol. Catal. A-Chem. 395 (2014) 486–493.
[31] F. Cavani, S. Guidetti, L. Marinelli, M. Piccinini, E. Ghedini, M. Signoretto, Appl. Catal. B 100 (2010) 197–204.
[32] P. Lauriol-Garbey, J. Millet, S. Loridant, V. Belliere-Baca, P. Rey, J. Catal. 281 (2011) 362–370.
[33] Y. Kim, K. Jung, E. Park, Appl. Catal. B 107 (2011) 177–187.
[34] Y. Kim, S. You, K. Jung, E. Park, Bull. Korean Chem. Soc. 33 (2012) 2369–2377.
[35] C. Carrico, F. Cruz, M. Santos, H. Pastore, H. Andrade, A. Mascarenhas, Micropor. Mesopor. Mater. 181 (2013) 74–82.
[36] P. Lauriol-Garbey, G. Postole, S. Loridant, A. Auroux, V. Belliere-Baca, P. Rey, J. Millet, Appl. Catal. B 106 (2011) 94–102.
[37] R. Liu, T. Wang, D. Cai, Y. Jin, Ind. Eng. Chem. Res. 53 (2014) 8667–8674.
[38] J.L. Dubois, C.H. Duquenne, W. Hoelderich, J. Kervennal, EP06/000736, in: Arkema (Ed.), France, (2006).
[39] J.L. Dubois, C. Duquenne, W. Hoelderich, EP06/000735, USA, (2006).
[40] J.L. Dubois, C. Duquenne, W. Hoelderich, EP1874720, in: Arkema (Ed.), France, (2008).
[41] W. Hoelderich, A. Ülgen, DE 10 2008 027350–3, 2008.
[42] W.F. Hoelderich, A. Ülgen, DE 10 2008 031828–0, 2008.
[43] H. Atia, U. Armbruster, A. Martin, J. Catal. 258 (2008) 71–82.
[44] W. Suprun, M. Lutecki, T. Haber, H. Papp, J. Mol. Catal. A-Chem. 309 (2009) 71–78.
[45] S. Chai, H. Wang, Y. Liang, B. Xu, J. Catal. 250 (2007) 342–349.
[46] P. Lauriol-Garbey, G. Postole, S. Loridant, A. Auroux, V. Belliere-Baca, P. Rey, J. Millet, Appl. Catal. B-Environ. 106 (2011) 94–102.
[47] N. Shiju, D. Brown, K. Wilson, G. Rothenberg, Top. Catal. 53 (2010) 1217–1223.
[48] M. Massa, A. Andersson, E. Finocchio, G. Busca, J. Catal. 307 (2013) 170–184.
[49] Y.Y. Lee, K.A. Lee, N.C. Park, Y.C. Kim, Catal. Today 232 (2014) 114–118.
[50] J. Jehng, I. Wachs, ACS Symp. Ser. 437 (1990) 232–242.
[51] S. Das, M. Bhunia, A. Sinha, A. Bhaumik, ACS Catal. 1 (2011) 493–501.
[52] M. Paul, N. Pal, B. Rana, A. Sinha, A. Bhaumik, Catal. Commun. 10 (2009) 2041–2045.
[53] M. Anilkumar, W. Hoelderich, J. Catal. 293 (2012) 76–84.
[54] M. Anilkumar, W. Hoelderich, Catal. Today 198 (2012) 289–299.
[55] M. Di Serio, R. Turco, P. Pernice, A. Aronne, F. Sannino, E. Santacesaria, Catal. Today 192 (2012) 112–116.
[56] H. Bosman, E. Kruissink, J. Vanderspoel, F. Vandenbrink, J. Catal. 148 (1994) 660–672.
[57] J. Iglesias, J. Melero, L. Bautista, G. Morales, R. Sanchez-Vazquez, M. Andreola, A. Lizarraga-Fernandez, Catal. Today 167 (2011) 46–55.
[58] S. Dzwigaj, Y. Millot, C. Methivier, M. Che, Micropor. Mesopor. Mater. 130 (2010) 162–166.
[59] A. Aronne, E. Marenna, V. Califano, E. Fanelli, P. Pernice, M. Trifuoggi, A. Vergara, J. Sol–Gel Sci. Technol. 43 (2007) 193–204.
[60] T. Onfroy, O. Manoilova, S. Bukallah, D. Hercules, G. Clet, M. Houalla, Appl. Catal. A 316 (2007) 184–190.
[61] L. Burcham, J. Datka, I. Wachs, J. Phys. Chem. B 103 (1999) 6015–6024.
[62] P. Burke, E. Ko, J. Catal. 129 (1991) 38–46.
[63] I. Wachs, J. Jehng, G. Deo, H. Hu, N. Arora, Catal. Today 28 (1996) 199–205.
[64] I. Wachs, Catal. Today 27 (1996) 437–455.
[65] J. Jehng, I. Wachs, J. Phys. Chem. 95 (1991) 7373–7379.
[66] V. Braga, J. Dias, S. Dias, J. de Macedo, Chem. Mater. 17 (2005) 690–695.
[67] J. Jehng, I. Wachs, E. Ko, Catal. Today 8 (1990) 37–55.
[68] J. Jehng, I. Wachs, J. Mol. Catal. 67 (1991) 369–387.
[69] K. Tanaka, A. OzakiI, J. Catal. 8 (1967) 1–7.
[70] Q. Xia, Q. Cuan, X. Liu, X. Gong, G. Lu, Y. Wang, Angew. Chem. Int. Ed. 53 (2014) 9755–9760.
[71] R. Pittman, A. Bell, J. Phys. Chem. 97 (1993) 12178–12185.
[72] S. Damyanova, P. Grange, B. Delmon, J. Catal. 168 (1997) 421–430.
[73] H. Bosman, A. Pijpers, A. Jaspers, J. Catal. 161 (1996) 551–559.
[74] A. Ramanathan, M. Villalobos, C. Kwakernaak, S. Telalovic, U. Hanefeld, Chem. -Eur. J. 14 (2008) 961–972.
[75] F. Verpoort, G. Dedoncker, A. Bossuyt, L. Fiermans, L. Verdonck, J. Electron. Spectrosc. Relat. Phenom. 73 (1995) 271–281.
[76] E. Pereira, M. Pereira, Y. Lam, C. Perez, M. Schmal, Appl. Catal A 197 (2000) 99–106.
[77] M. de Pietre, L. Almeida, R. Landers, R. Vinhas, F. Luna, React. Kinet. Mech. Catal. 99 (2010) 269–280.
[78] J. Yan, G. Wu, N. Guan, L. Li, Appl. Catal. B 152–153 (2014) 280–288.
[79] L. Dragone, P. Moggi, G. Predieri, R. Zanoni, Appl. Surf. Sci. 187 (2002) 82–88.
[80] E. Rodriguez-Castellon, A. Jimenez-Lopez, P. Maireles-Torres, D. Jones, J. Roziere, M. Trombetta, G. Busca, M. Lenarda, L. Storaro, J. Solid State Chem. 175 (2003) 159–169.
[81] R. Ladera, E. Finocchio, S. Rojas, J. Fierro, M. Ojeda, Catal. Today 192 (2012) 136–143.
[82] G. Busca, Catal. Today 41 (1998) 191–206.
[83] J. Datka, A. Turek, J. Jehng, I. Wachs, J. Catal. 135 (1992) 186–199.
[84] G. Connell, J. Dumesic, J. Catal. 105 (1987) 285–298.
[85] M. Zaki, G. Hussein, S. Mansour, H. Elammawy, J. Mol. Catal. 51 (1989) 209–220.
[86] M. Zaki, M. Hasan, F. Al-Sagheer, L. Pasupulety, Colloids Surf. A 190 (2001) 261–274.

[87] D. Stosic, S. Bennici, S. Sirotin, P. Stelmachowski, J. Couturier, J. Dubois, A. Travert, A. Auroux, Catal. Today 226 (2014) 167–175.
[88] S. Maurer, E. Ko, J. Catal. 135 (1992) 125–134.
[89] H. Yoshida, T. Tanaka, T. Yoshida, T. Funabiki, S. Yoshida, Catal. Today 28 (1996) 79–89.
[90] C. Garcia-Sancho, I. Agirrezabal-Telleria, M. Guemez, P. Maireles-Torres, Appl. Catal. B 152 (2014) 1–10.
[91] D. Stosic, S. Bennici, V. Rakic, A. Auroux, Catal. Today 192 (2012) 160–168.
[92] K. Nakajima, Y. Baba, R. Noma, M. Kitano, J. Kondo, S. Hayashi, M. Hara, J. Am. Chem. Soc. 133 (2011) 4224–4227.
[93] W. Fan, Q. Zhang, W. Deng, Y. Wang, Chem. Mater. 25 (2013) 3277–3287.
[94] I. Bassan, D. Nascimento, R. San Gil, M. da Silva, C. Moreira, W. Gonzalez, A. Faro, T. Onfroy, E. Lachter, Fuel Process. Technol. 106 (2013) 619–624.
[95] C. Garcia-Sancho, R. Moreno-Tost, J. Merida-Robles, J. Santamaria-Gonzalez, A. Jimenez-Lopez, P. Maireles-Torres, Appl. Catal. B 108 (2011) 161–167.
[96] W. Suprun, M. Lutecki, R. Glaser, H. Papp, J. Mol. Catal. A: Chem. 342–43 (2011) 91–100.
[97] G. Raju, P.S. Reddy, B.M. Reddy, Open Catal. J. 4 (2011) 83–87.
[98] A. Kinage, P. Upare, P. Kasinathan, Y. Hwang, J. Chang, Catal. Commun. 11 (2010) 620–623.
[99] G. Foo, D. Wei, D. Sholl, C. Sievers, ACS Catal. 4 (2014) 3180–3192.
[100] J. Copeland, X. Shi, D. Sholl, C. Sievers, Langmuir 29 (2013) 581–593.
[101] J. Copeland, I. Santillan, S. Schimming, J. Ewbank, C. Sievers, J. Phys. Chem. C 117 (2013) 21413–21425.
[102] T. Laino, C. Tuma, A. Curioni, E. Jochnowitz, S. Stolz, J. Phys. Chem. A 115 (2011) 3592–3595.
[103] M. Nimlos, S. Blanksby, X. Qian, M. Himmel, D. Johnson, J. Phys. Chem. A 110 (2006) 6145–6156.
[104] S. Chai, H. Wang, Y. Liang, B. Xu, Green Chem. 9 (2007) 1130–1136.
[105] C. Jia, Y. Liu, W. Schmidt, A. Lu, F. Schuth, J. Catal. 269 (2010) 71–79.